How to cite: *Angew. Chem. Int. Ed.* **2020**, *59*, 12098–12104
International Edition: doi.org/10.1002/anie.202003637
German Edition: doi.org/10.1002/ange.202003637

VIP Adamantane Very Important Paper

Infrared Spectrum of the Adamantane$^+$–Water Cation: Hydration-Induced C–H Bond Activation and Free Internal Water Rotation

*Martin Andreas Robert George, Marko Förstel, and Otto Dopfer**

Abstract: *Diamondoid cations are reactive intermediates in their functionalization reactions in polar solution. Hydration is predicted to strongly activate their C–H bonds in initial proton abstraction reactions. To study the effects of microhydration on the properties of diamondoid cations, we characterize herein the prototypical monohydrated adamantane cation ($C_{10}H_{16}^+$–H_2O, Ad^+–W) in its ground electronic state by infrared photodissociation spectroscopy in the CH and OH stretch ranges and dispersion-corrected density functional theory (DFT) calculations. The water (W) ligand binds to the acidic CH group of Jahn–Teller distorted Ad^+ via a strong CH···O ionic H-bond supported by charge–dipole forces. Although W further enhances the acidity of this CH group along with a proton shift toward the solvent, the proton remains with Ad^+ in the monohydrate. We infer essentially free internal W rotation from rotational fine structure of the ν_3 band of W, resulting from weak angular anisotropy of the Ad^+–W potential.*

Introduction

Adamantane ($C_{10}H_{16}$, Ad) is the parent molecule of diamondoids, which are nanometer-sized H-passivated nanodiamonds.[1] These rigid and stress-free cycloalkanes and their derivatives have well-defined stable structures and thus are of interest in a variety of disciplines, with (potential) applications ranging from materials and polymer sciences, molecular electronics, medical sciences, and chemical synthesis to astrochemistry.[2] Specifically, radical cations of diamondoids are intermediates in the their functionalization reactions in polar solvents.[2d,3] Quantum chemical calculations predict a substantial activation and eventually rupture of the most acidic C–H bond in these radical cations caused by solvation with a few polar solvent molecules, such as water (H_2O, W) or acetonitrile.[2d,3] This appears to be the first step required for H substitution via a radical cation mechanism.

To understand the involved reaction mechanism at the molecular level, detailed knowledge of the interaction between the diamondoid radical cation and the solvent molecules is required. To this end, we characterize the interaction between Ad^+, the parent cation of the diamondoid family, and W ligands by 1) infrared photodissociation (IRPD) spectroscopy of mass-selected $(Ad–W_n)^+$ clusters generated in a molecular beam and 2) dispersion-corrected density functional theory (DFT) calculations. Herein, we report the results obtained for monohydrated Ad^+–W. Significantly, these results represent the first experimental (and in particular spectroscopic) characterization of any diamondoid cation interacting with a polar solvent.

The scarce knowledge of Ad^+ comes from photoelectron and fragmentation spectroscopy,[4] IR spectroscopy,[5] and calculations.[2d,3a,5,6] Neutral Ad has a structure with T_d symmetry, four equivalent CH groups, and six equivalent CH_2 groups (Figure 1).[7] Ionization from the fully occupied triply degenerate $(7t_2)^6$ HOMO leads to the Jahn–Teller distorted $^2A_1$ cation ground state with $(12e)^4(12a_1)^1$ configuration and C_{3v} symmetry.[5,6] Removal of the bonding electron leads to a pronounced elongation of one of the C–H bonds along the C_3 axis. This predicted activation has experimentally been probed in IRPD spectra of Ad^+–He_n and Ad^+–N_2 clusters via its unusually low C–H stretch frequency at 2600 cm^{-1}.[5] Similar C–H bond activation has more recently been observed for ionization of linear alkanes and their hydrated clusters.[8] The analysis of the IRPD spectrum of monohydrated Ad^+–W elucidates the interaction potential between Ad^+ and W with respect to the binding site, the strength and anisotropy of the interaction, and the magnitude of hydration-induced C–H bond activation.

Results and Discussion

The IRPD spectrum of mass-selected Ad^+–W clusters is measured in the W loss channel in a tandem quadrupole mass spectrometer coupled to an electron ionisation source using an optical parametric oscillator laser system,[9] a setup previously used to record IR spectra of hydrocarbon cation clusters.[5,10] The investigated range (2400–3900 cm^{-1}) covers the informative OH and CH stretch modes (ν_{OH}, $\nu_{CH(2)}$). Quantum chemical calculations are performed at the dispersion-corrected B3LYP-D3/cc-pVTZ level to elucidate the energetic, structural, electronic, and vibrational properties of Ad, Ad^+, and its Ad^+–W clusters.[11] Additional calculations at other DFT levels yield essentially the same results. Relative energies (E_e) and binding energies (D_e) are corrected for harmonic zero-point vibrational energies to derive E_0 and D_0.

The computed structures and scaled harmonic IR spectra of W, Ad, and Ad^+ shown in Figure 1, Figure 2, and Figure S1

[*] M. A. R. George, Dr. M. Förstel, Prof. Dr. O. Dopfer
Institut für Optik und Atomare Physik, Technische Universität Berlin
Hardenbergstrasse 36, 10623 Berlin (Germany)
E-mail: dopfer@physik.tu-berlin.de
Supporting information and the ORCID identification number(s) for the author(s) of this article can be found under: https://doi.org/10.1002/anie.202003637.

© 2020 The Authors. Published by Wiley-VCH Verlag GmbH & Co. KGaA. This is an open access article under the terms of the Creative Commons Attribution Non-Commercial License, which permits use, distribution and reproduction in any medium, provided the original work is properly cited, and is not used for commercial purposes.

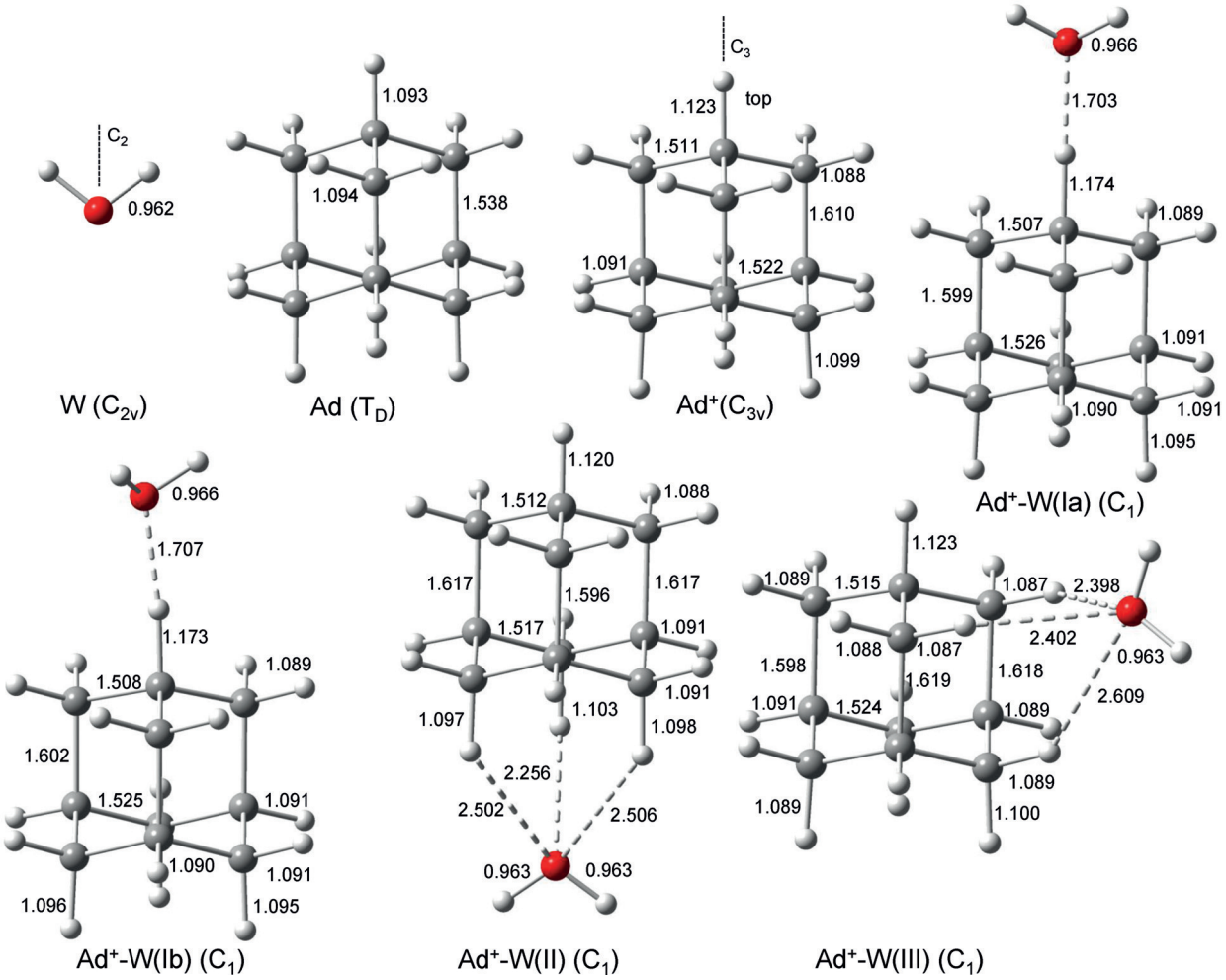

Figure 1. Calculated equilibrium structures (in [Å]) of W, Ad (T_d), Ad^+ (C_{3v}), Ad^+–W(**Ia/b-III**) in their ground electronic state (B3LYP-D3/cc-pVTZ). Further details are available in Figure S1. Red O, gray H, white H.

in the Supporting Information agree well with available computational and experimental data,[2d,3a,5,6,12] indicating that the B3LYP-D3/cc-pVTZ level describes the monomer units well. Ionization of Ad ($^1A_1$, T_d) into its ground electronic state results from removal of a bonding electron from the t_2 orbital, giving rise to Jahn–Teller distortion in the resulting $^2A_1$ state with C_{3v} symmetry.[5] According to the shape of the a_1 orbital (Figure S2), the major structural impact of ionization are an elongation of the three C–C bonds parallel to the C_3 axis by 72 mÅ (the other C–C bonds contract by 27 mÅ and 16 mÅ) and a drastic elongation of the C–H bond on the C_3 axis by 30 mÅ. This C–H bond located at the top of Ad^+ becomes very acidic and carries the largest positive partial charge of all protons (354 me, Figure S3). As a result, the corresponding $\nu_{CH}{}^t$ frequency is rather low (2606 cm^{-1}), in agreement with experiment (Figure 2).[5]

The Jahn–Teller distorted Ad^+ cation offers three attractive binding sites for W, which can be attached to the top (**Ia/b**), the bottom (**II**), and the side (**III**) of the distorted Ad^+ tetrahedron (Figure 1). All structures have a favourable charge–dipole configuration, with the O atom of W pointing toward the Ad^+ cation. Because the ionization energy of Ad is much lower than that of W (9.25 vs. 12.6 eV)[12] and the computed proton affinity of the adamantyl radical ($C_{10}H_{15}$) is much higher than that of W (PA = 868 vs. 691 kJ mol^{-1}),[12] neither charge nor proton transfer occurs upon monohydration, justifying the notation of Ad^+–W in the ground electronic state. The computed linear IR spectra of all Ad^+–W isomers in the $\nu_{OH/CH(2)}$ range are compared in Figure 2 to that of W and Ad^+ (Table 1 and Figure S1). In the Ad^+–W(**Ia**) global minimum, W forms a strong and nearly linear CH···O ionic H-bond to the acidic CH group at the top of Ad^+, with a high binding energy of $D_0 = 45.6$ kJ mol^{-1} and a short intermolecular distance of $R_{CH\cdots O} = 1.703$ Å. The **Ia** structure is similar to the one calculated previously at the lower B3LYP/6-31G* level.[3a] W is not directly aligned along the C_3 rotational axis, with a CH···O bond angle of $\theta_{CHO} = 170.2°$ and an angle of $\theta_{C2} = 46.2°$ between the C_2 axis (*b* axis) of W and the intermolecular axis, indicating that the CH group binds to one of the two lone pairs of W. Upon hydration, the acidic C–H donor bond is further elongated by 49 mÅ compared to Ad^+ ($r_{CH} = 1.174$ Å), leading to substantial additional activation. As a result, its bound CH stretch frequency $\nu_{CH}{}^t$ shifts down from 2606 to 2033 cm^{-1} (outside

 © 2020 The Authors. Published by Wiley-VCH Verlag GmbH & Co. KGaA, Weinheim

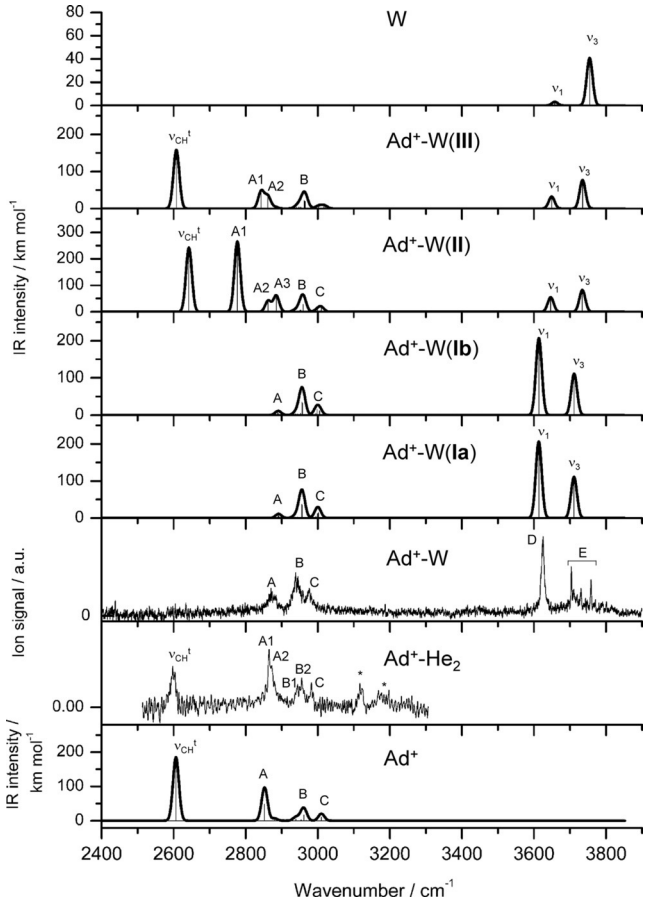

Figure 2. IRPD spectra of Ad^+–W and Ad^+–He_2 [5] compared to linear and scaled harmonic IR absorption spectra of Ad^+, W, and Ad^+–W(**Ia**/**b**-**III**) calculated at the B3LYP-D3/cc-pVTZ level (scaling factor 0.963). The positions of the transition observed in the IRPD spectrum of Ad^+–W (A–E) and their vibrational assignment are listed in Table 1. Band E consists of three sharp Q branches owing to internal W rotation.

the scanning range) along with a drastic enhancement in the IR intensity. This massive redshift of 573 cm^{-1} (or 22%) illustrates that IR spectroscopy is a sensitive probe for chemical bond activation. The substantial charge transfer of 124 me from Ad^+ to W upon formation of the CH···O H-bond (Figure S3) is also visible in the HOMO orbital (Figure S2). It results in an elongation of the O–H bonds ($\Delta r_{OH} = 4$ mÅ), with a concomitant redshift in the free OH stretch frequencies ($-\Delta\nu_{1/3} = 45/43$ cm^{-1}) and a strong IR enhancement, as is typical for cation–W dimers.[9b,10h,i,13] Apart from the acidic CH group, monohydration has only a minor impact on the structure of the remaining Ad^+ cage ($\Delta r_{CC} < 14$ mÅ, $\Delta r_{CH} \leq 4$ mÅ). As a result, the remaining three CH and twelve CH_2 stretch frequencies do not change much ($\Delta\nu_{CH(2)} \leq 10$ cm^{-1}), with the notable exception of the three symmetric CH_2 stretches at the bottom of the cage, $\nu_{CH2}(s)^b$. These are blueshifted by 27–40 cm^{-1} and strongly suppressed in IR intensity by monohydration
(band A), in line with the computed C–H bond contraction (4 mÅ). Band C, with a convoluted maximum at 3000 cm^{-1}, is composed of the three high-frequency antisymmetric CH_2 stretches of the top of Ad^+, $\nu_{CH2}(a)^t$, slightly redshifted from those of Ad^+. The most intense band B in the free CH(2) stretch range peaking at 2956 cm^{-1} contains the three bottom CH stretches, $\nu_{CH}{}^b$, and the remaining three $\nu_{CH2}(s)^t$ and three $\nu_{CH2}(a)^b$ modes (strongly coupled), whereby most of the intensity is coming from two modes at 2956 and 2957 cm^{-1}, nearly unshifted from those of Ad^+ (−5 cm^{-1}).

Internal rotation of the Ad^+ cage of **Ia** by approximately 60° around the C_3 axis results in a second and essentially isoenergetic isomer **Ib** ($E_0 = 0.26$ kJ mol^{-1}), with very similar structural, energetic, and vibrational properties as **Ia** (Figure 1, Figure 2, Figure S1, Table 1). Its CH···O H-bond is characterized by $D_0 = 45.3$ kJ mol^{-1}, $R_{CH\cdots O} = 1.71$ Å, $\theta_{CHO} = 170.3°$, $\theta_{C2} = 46.0°$, and $\Delta q = 123$ me. The activation of the acidic C–H bond is similar as in **Ia** ($r_{CH} = 1.173$ Å, $\nu_{CH} = 2040$ cm^{-1}), and also the properties of W are comparable.

The potential for internal rotation of Ad^+ around its C_3 axis has three equivalent global minima **Ia** ($E_0 = E_e = 0$) at 0°, 120°, and 240°, and three local minima **Ib** at approximately 60°, 180°, and 300° ($E_0 = 0.26$ kJ mol^{-1}, $E_e = 0.03$ kJ mol^{-1}), which are separated by six low-energy transition states **TS1** at approximately 30°, 90°, 150°, 210°, 270°, and 330° with a barrier of $V_b = 0.40$ kJ mol^{-1} above **Ia** ($\theta_{CHO} = 168.0°$, $\theta_{C2} = 46.2°$, $R_{CH\cdots O} = 1.707$ Å, $r_{CH} = 1.173$ Å, Figure S4). There are further low-energy **TS2** at $V_b = 2.68$ kJ mol^{-1} ($\theta_{CHO} = 177.6°$, $R_{CH\cdots O} = 1.735$ Å, $r_{CH} = 1.163$ Å, Figure S4), which connect **Ia** and **Ib** minima separated by 180° via a flipping motion of W, whereby the CH group changes the bonding from one to the other lone pair of W. In contrast to **Ia**/**b** and **TS1**, the *b* axis of W is (nearly) parallel to the intermolecular axis of Ad^+ ($\theta_{C2} = 1.5°$), so that the barrier for internal W rotation around this axis approaches zero ($V_b < 10$ cm^{-1}), while those for **Ia**/**b** are rather high ($V_b = 27$ kJ mol^{-1}, Figure S5) because of steric hindrance with the Ad^+ cage and the rupture of the H-bond to the lone pair. In conclusion, the Ad^+–W potential at the top of Ad^+ is rather flat, and the calculations predict four non-equivalent low-energy stationary points (**Ia**/**b**, **TS1**/**2**), with essentially the same energy and IR spectra in the $\nu_{OH/CH(2)}$ range (Figures 2 and S6), so that they cannot by distinguished by the measured IRPD spectrum.

In the low-energy isomers **II** and **III** ($E_0 = 3.50$ and 4.79 kJ mol^{-1}), W does not bind to Ad^+ via a single, strong, and nearly linear CH···O bond to the acidic CH proton but forms instead three nonlinear CH^+···O H-bonds to three different CH_2 groups at either the side or the bottom of the Ad^+ cage. Although the individual CH···O contacts in **II** and **III** are much longer than those in **Ia** and **Ib** (2.26–2.61 vs. ca. 1.71 Å) and charge transfer from Ad^+ to W is largely reduced (from 124 to 23 and 9 me), their binding energies of $D_0 = 42.1$ and 40.8 kJ mol^{-1} remain comparable at the B3LYP-D3/cc-pVTZ level. The Ad^+···W bonding in **II** and **III** is essentially based on charge–dipole forces and has only little contribution from H-bonding. As a result of the minor charge transfer, the O–H bonds of W are much less affected ($\Delta r_{OH} = 1$ mÅ), leading to smaller red shifts ($-\Delta\nu_{1/3} = 12/20$ and 9/19 cm^{-1}) and lower IR activity (Figure 2, Table 1). While the IR spectra of **Ia** and **Ib** are quite similar in both the investigated CH and OH stretch ranges, those of **II** and **III** are rather different. Significantly, the acidic free CH stretch of Ad^+ at 2606 cm^{-1} remains for **II** and **III** in this frequency range ($\nu_{CH}{}^t = 2642$ and

 © 2020 The Authors. Published by Wiley-VCH Verlag GmbH & Co. KGaA, Weinheim

Table 1: Computed vibrational frequencies (in cm^{-1}, B3LYP-D3/cc-pVTZ) of Ad^+, W, and Ad^+–W(**Ia/b**) and experimental values of Ad^+He_2 and Ad^+–W.[a]

Mode[b]	Ad^+ (C_{3v})	W (C_{2v})	Ad^+–W(**Ia**)	Ad^+–W(**Ib**)	Ad^+–He_2 exp[c]	Ad^+–W exp
$\nu_{CH}{}^t$	2606 (185,a_1)		2033 (3016)	2040 (2994)	2600	
$\nu_{CH2}(s)^b$	2852 (48,e)		2890 (6)	2889 (7)	2868 A1	2875 (23) A
$\nu_{CH2}(s)^b$	2852 (48,e)		2892 (5)	2892 (5)	2868 A1	2875 (23) A
$\nu_{CH2}(s)^b$	2880 (7,a_1)		2907 (0.2)	2906 (0.6)	2883 A2	2875 (23) A
$\nu_{CH}{}^b$	2939 (5,e)		2937 (3)	2935 (2)	2941 B1	
$\nu_{CH}{}^b$	2939 (5,e)		2938 (3)	2938 (4)	2941 B1	
$\nu_{CH}{}^b$	2948 (0.1,a_1)		2944 (3)	2944 (4)		
ν_{CH2}	2953 (2,e)		2949 (1)	2949 (1)		
ν_{CH2}	2953 (2,e)		2950 (0.6)	2950 (1)		
ν_{CH2}	2955 (2,a_1)		2951 (2)	2952 (5)		
ν_{CH2}	2961 (16,e)		2956 (37)	2956 (35)	2954 B2	2942 (20) B
ν_{CH2}	2961 (16,e)		2957 (35)	2957 (32)	2954 B2	2942 (20) B
ν_{CH2}	2968 (1,a_1)		2962 (1)	2962 (2)		
$\nu_{CH2}(a)^t$	3005 (0,a_2)		2995 (4)	2994 (4)		
$\nu_{CH2}(a)^t$	3010 (10,e)		3000 (12)	2998 (15)	2981 C	2976 (13) C
$\nu_{CH2}(a)^t$	3010 (10,e)		3002 (15)	3005 (12)	2981 C	2976 (13) C
ν_1		3658 (3,a_1)	3613 (206)	3614 (207)		3625 (13) D
ν_3		3754 (41,b_1)	3711 (111)	3711 (111)		3717[d] E

[a] For calculated harmonic frequencies (scaled by 0.963), IR intensities (in km mol^{-1}) and symmetry species are listed in parentheses. For experimental values the width of the band is given in parentheses. [b] The six ν_{CH2} modes are a mixture of $\nu_{CH2}(s)^t$ and $\nu_{CH2}(a)$ for **Ia/b**. [c] Ref. [5]. [d] Band origin ν_0.

2607 cm^{-1}) with high IR activity, because this bond is little affected by hydration at the side and bottom of Ad^+ ($\Delta r_{CH} \leq$ 5 mÅ). On the other hand, formation of the three CH···O contacts in **II** shifts the corresponding bonded ν_{CH2} mode down to 2776 cm^{-1} and its high IR activity makes this band the most intense transition (A1). In the IR spectra of both **II** and **III**, further ν_{CH2} frequencies shift down to well below 2900 cm^{-1} (A1-A3) with enhanced IR activity generating a characteristic fingerprint. Bands B and C remain rather unchanged from those of **Ia/b**. The transition states for interconverting **II/III** into **Ia/b** are quite high (16.1/14.7 kJ mol^{-1}) so that **II/III** may be trapped in their deep minima in the supersonic expansion.

The structures, energies, and IR spectra computed at the other DFT levels yield the same qualitative picture (Table S2, Figure S7), with very similar energies for the nearly isoenergetic **Ia/b** minima ($\Delta E_0 \leq 0.5$ kJ mol^{-1}), a substantial gap to **II** and **III** (4–13 kJ mol^{-1}), and the same IR spectral pattern.

In Figure 2, we show the IRPD spectrum of Ad^+–W to the linear IR absorption spectra computed for Ad^+, W, and the four Ad^+–W isomers **Ia**, **Ib**, **II**, and **III**. For comparison, we also include the IRPD spectrum of Ad^+–He_2 reported previously, which provides a close approximation to the spectrum of bare Ad^+ due to the weak bonding of He ($D_0 <$ 1 kJ mol^{-1}).[5] The IRPD spectrum of Ad^+–W reveals five vibrational transitions A–E, and their positions, widths, and vibrational and isomer assignments are listed in Table 1. The bands A–C occurring in the CH(2) stretch range at 2875, 2942, and 2976 cm^{-1} with widths of 13–23 cm^{-1} show only minor shifts from the corresponding bands of Ad^+–He_2 at 2868/2883 (A1/A2), 2941/2954 (B1/B2), and 2981 (C) cm^{-1} ($\Delta\nu < 6$ cm^{-1} for the band centers), although the latter spectrum shows higher spectral resolution owing to colder ions resulting from the smaller D_0 value. The stronger interaction with W changes the relative intensities of these bands. In addition, the intense band at $\nu_{CH}{}^t = 2600$ cm^{-1} assigned to the acidic CH group of Ad^+ is shifted away from the investigated spectral range, providing the first strong experimental evidence for the formation of a CH···O H-bond in Ad^+–W (isomer **I**). Finally, two new transitions D and E appear in the Ad^+–W spectrum at 3625 and 3717 cm^{-1}, which are readily assigned to the free OH stretch modes of W ($\nu_{1/3}$). The magnitude of their redshifts from bare W ($-\Delta\nu_{1/3} = 32/39$ cm^{-1}) and their relative intensities are indicative of a strongly bonded cation–dipole structure. While the unresolved ν_1 band (D) has only a slightly smaller width than the partly unresolved ν_{CH} bands (13 vs. 20–25 cm^{-1}), the ν_3 band (E) shows rotational substructure with narrow equidistant Q branches at 3703, 3731, and 3759 cm^{-1}, with a width of 3–4 cm^{-1} and a spacing of around 28 cm^{-1}, indicative of internal rotation of the W ligand. Interestingly, the two bands marked by asterisks in the Ad^+–He_2 spectrum (Figure 2) assigned to overtone and/or combination bands[5] disappear in the Ad^+–W spectrum because of the significant impact of W on the Ad^+ cage.

Comparison of the IRPD spectrum of Ad^+–W to the calculated ones unambiguously shows that W binds to the acidic CH group by forming a CH···O ionic H-bond, with convincing agreement for isomers **Ia/b** concerning both positions and relative intensities of all transitions observed (with maximum, mean, and summed deviations of 26, 15, and 14 cm^{-1}). Moreover, the shifts and intensity changes of the $\nu_{CH(2)}$ bands A–C predicted for He→W substitution are well reproduced by experiment. The match between predicted and measured $\nu_{CH(2)}$ bands indicates that anharmonic couplings between CH stretch fundamentals and CH bend overtones are not important for this system (at least at the achieved spectral resolution). On the other hand, the most intense transitions of the higher energy isomers **II** and **III** between 2600 and 2700 cm^{-1} are absent in the measured spectrum and also their predicted $\Delta\nu_{1/3}$ redshifts are much smaller than the observed ones. In addition, the computed ν_1 frequencies of **Ia/b** and **II/III** differ by as much as about 35 cm^{-1} and no such splitting is observed experimentally. Consequently, the IRPD spectrum of Ad^+–W is solely assigned to **Ia/b**, while **II** and **III** are below the detection limit (consistent with their lower stability, population estimated as $< 3\%$ of **Ia/b** by considering the achieved signal-to-noise ratio and the computed IR intensities). Because **Ia** and **Ib** have very similar energies and IR spectra, the IRPD spectrum is of insufficient resolution to exclude one or the other. Indeed, the computations predict low barriers for their interconversion (**Ia** ↔ **Ib**) so that the zero-point vibrational level lies probably above these barriers

 © 2020 The Authors. Published by Wiley-VCH Verlag GmbH & Co. KGaA, Weinheim

leading to a vibrationally averaged structure between the two nonequivalent triply degenerate minima, denoted structure **I**. The binding energy of Ad^+–W(**Ia**) computed at the highest level (B3LYP-D3/aug-cc-pVTZ) is $D_0 = 35.4\ kJ\,mol^{-1}$ or $2960\ cm^{-1}$ (Table S2), indicating that single-photon IRPD in the CH and OH stretch ranges is feasible for cold cluster ions in the ground or low-energy vibrationally excited states.

Interestingly, the ν_3 band (E) of Ad^+–W shows rotational fine structure. Three narrow Q branches spaced by $28\ cm^{-1}$ indicate an effective internal rotational constant of $A_{eff} = 14\ cm^{-1}$ (Figure S8). The rotational constants of W ($A_W = 27.88$, $B_W = 14.52$, and $C_W = 9.28\ cm^{-1}$)[12] suggest to assign this spectral feature to nearly free internal rotation of the W subunit around its *b* axis because $B_W \approx A_{eff}$. The observed A_{eff} value is slightly smaller than B_W due to the presence of the heavy Ad^+ unit and/or a small nonvanishing barrier. The selection rules for the observed Q branches of the perpendicular ν_3 component are $\Delta J = 0$ and $\Delta k = \pm 1$, where *J* is the total rotational quantum number of Ad^+–W and *k* the internal rotational quantum number for W rotation. According to the Pauli principle for fermions, even and odd *k* rotational levels are combined with symmetric (triplet, $I = 1$, $M_I = 0$ and ± 1) and antisymmetric (singlet, $I = 0$, $M_I = 0$) nuclear spin wave functions for exchange of the two equivalent protons (nuclear spin $i = 1/2$), with nuclear spin statistical weights of 3:1, respectively. As a result, supersonic cooling freezes the *k* level populations down to $k = 0/1$ for $k =$ even/odd levels with a weight of 1/3. The three remaining ^{P}Q and ^{R}Q branches (in the notation $^{\Delta k}\Delta J$ with $\Delta J = 0$) expected for low temperature are then those originating from $k = 0$ ($1 \leftarrow 0$, weak) and $k = 1$ ($0 \leftarrow 1$, $2 \leftarrow 1$, strong), and these are indeed the detected Q branches (Figure S8, Table S3). From the absence of any transition originating from $k = 2$, an upper limit for the (rotational) temperature is estimated as $T = 70$ K. The ν_3 band origin (ν_0) occurs at the $0 \leftarrow 0$ subband, which is forbidden for a purely perpendicular transition but becomes weakly allowed for a hybrid and indeed we observe a weak signal where the parallel component is expected. The ν_1 band does not exhibit any Q branches because the selection rules for this mostly parallel transition are $\Delta J = \pm 1$ and $\Delta k = 0$, and the resulting P and R branches of the overall end-over-end rotation of Ad^+–W cannot be resolved due to the small rotational constants ($A_e = 0.056$, $B_e = 0.028$, $C_e = 0.028\ cm^{-1}$ for **Ia**).

According to the calculations, the equilibrium structures **Ia** and **Ib** have a too high barrier for W rotation around its *b* axis ($V_b \approx 27\ kJ\,mol^{-1}$ or $2250\ cm^{-1}$, Figure S4) to explain the observed (nearly) free rotation because of steric hindrance. Hence, the small computed barriers between the three **Ia** and **Ib** minima at **TS1** and also **TS2** suggest that in the effective vibrationally averaged structure, the angle between the *b* axis of W and the C_3 axis of Ad^+ is much smaller than computed for **Ia**/**b**. For example, the tilt angle for **TS2** is 1.5° leading to a negligible rotation barrier. In this scenario, the W ligand experiences only a low effective anisotropy for rotation around its *b* axis because the three CH_2 groups at the top of Ad^+ are far away, yielding low V_3 and V_6 parameters for an effective one-dimensional internal rotation potential with threefold symmetry. Calculations at other DFT levels confirm that that the nonrigidity of W above the Ad^+ cation is the reason for observing nearly free internal rotation (and not a wrongly computed equilibrium structure for **Ia**/**b**). We note that free internal W rotation has previously been observed for a number of cation–W clusters (A^+–W), including small inorganic (e.g., $A^+ = NH_4^+$)[14] and atomic metal cations (e.g., $Cr^{+/2+}$).[15] So far, free internal W rotation has not been identified for clusters with hydrocarbon cations, although the IR spectra of the ν_3 bands of A^+–W with A = pentane[8b] and protonated benzonitrile[13b] with linear CH···O and NH···O ionic H-bonds show related spectral features (which were however not analysed). In A^+–W clusters with aromatic hydrocarbons (e.g., A = benzene or naphthalene), internal W rotation is locked by bifurcated CH···O bonding to both lone pairs of W.[10h,i] The reason why the internal rotation in Ad^+–W is (nearly) free is because W experiences essentially an almost spherical Ad^+ cation connected by a single nearly linear CH···O ionic H-bond.

The C–H bond of Ad along the C_3 axis becomes strongly elongated upon ionization (by 30 mÅ) and gets further activated by monohydration (by 51 mÅ) upon formation of the strong CH···O H-bond. Although the proton still remains with Ad^+, the large destabilization of the C–H bond is indicated by the large redshift of ν_{CH}^t down to around $2040\ cm^{-1}$. Thus, a single W ligand is not sufficient for driving the intracluster proton transfer, which is necessary for the functionalization reaction of Ad in a polar solvent. This experimental result is consistent with our and previous DFT calculations.[2d,3a] It is also in line with the thermochemical expectation from the proton affinities of $C_{10}H_{15}$ (computed as $PA = 868\ kJ\,mol^{-1}$), which is much higher than that of W ($691\ kJ\,mol^{-1}$).[12] From the proton affinities of W_2 and W_3 (808 an 862 $kJ\,mol^{-1}$),[16] we expect proton transfer to solvent to occur in $(Ad–W_n)^+$ clusters with $n = 2$–3. Such a strong activation of the aliphatic CH groups upon monohydration of this prototypical cycloalkane cation has previously been noted for linear alkane cations such as pentane (C_5H_{12}).[8b] In $(C_5H_{12}–W)^+$, the proton in the C···H$^+$···O bond is already closer to O than to C, indicating that the C–H bond in linear $C_5H_{12}^+$ is even more acidic than in cyclic Ad^+. Interestingly, the more fundamental $(CH_4–W)^+$ cation has the proton-transferred form $CH_3–H^+W$ with an OH···C ionic H-bond ($R_{OH\cdots C} = 1.726$ Å, $D_0 = 69.8\ kJ\,mol^{-1}$, Figure S10), because the PA of CH_3 is much lower than that of W (542 vs. $695\ kJ\,mol^{-1}$) leading to complete and barrierless intracluster proton transfer from CH_4^+ to W. This result is consistent with the corresponding exothermic ion–molecule reaction of CH_4^+ with W (or CH_4 with W^+) resulting in CH_3 and H^+W.[17]

Finally, we compare the strength of the CH···O ionic H-bond in Ad^+–W to those in related hydrocarbon radical cations studied recently using the same computational and spectroscopic approach. The bifurcated CH···O H-bond observed in polycyclic aromatic hydrocarbons (PAH) are comparable to those in Ad^+–W ($D_0 = 35.4\ kJ\,mol^{-1}$, $R_{CH\cdots O} = 1.17$ Å, B3LYP-D3/aug-cc-pVTZ), such as benzene$^+$–W ($38.4\ kJ\,mol^{-1}$, 2.40 Å) and naphthalene$^+$–W ($33.2\ kJ\,mol^{-1}$, 2.372 Å), although their H-bonds are much longer and involve less charge transfer to W (10 and 8 me vs. 112 me).[10i] Consequently, they exhibit a much smaller C–H

 © 2020 The Authors. Published by Wiley-VCH Verlag GmbH & Co. KGaA, Weinheim

bond elongation (2 and 1 mÅ vs. 42 mÅ). Protonated H^+PAH–W cations have similarly strong bifurcated CH···O H-bonds, as for example in H^+naphthalene–W (31.7 kJ mol^{-1}, 2.42 Å) with small charge transfer (11 me) and minor C–H bond activation (1 mÅ).[13a] On the other hand, the linear C···H^+···O H-bond in $(C_5H_{12}–W)^+$ is much stronger than in Ad^+–W, which is closer to a C_5H_{11}–H^+W structure, with an enormous redshift of ν_{CH} down to 1300 cm^{-1} and larger redshifts in the free OH stretch modes.[8b]

Conclusion

In summary, the intermolecular interaction between W and the Jahn–Teller distorted Ad^+ radical cation is characterized by IRPD spectroscopy and DFT calculations of Ad^+–W to investigate the C–H bond activation of this prototypical diamondoid cation upon monohydration. Significantly, these spectra provide the first spectroscopic information of any microhydrated diamondoid cation cluster, and thus result in a first impression of activation of their C–H bonds upon solvation with a polar solvent at the molecular level. The salient results may be summarized as follows. The IRPD spectrum of Ad^+–W in the CH and OH stretch range provides a clear picture of both the site and strength of monohydration. The W ligand binds with one of its lone pairs in a strong, short, and nearly linear CH···O ionic H-bond (1.70 Å) to the single acidic CH group of the Jahn–Teller distorted Ad^+ cation (isomers **Ia/b**), with a calculated binding energy of $D_0 = 45$ kJ mol^{-1}. Other isomers with other W binding sites at the side and bottom of the Ad^+ cage (**II**, **III**) and multiple CH···O contacts to three CH_2 groups are only slightly less stable ($\Delta E_0 \leq 5$ kJ mol^{-1}) but not observed experimentally. The potential of Ad^+–W is rather flat near the global minimum leading to a highly fluxional bonding with little angular anisotropy. For example, the triply degenerate and nearly isoenergetic **Ia/b** minima with an energy difference of only $E_0 = 0.3$ kJ mol^{-1} are separated by low barriers ($V_b \leq 3$ kJ mol^{-1}), and also structures with almost parallel C_2 and C_3 axes of W and Ad^+ are very low in energy (< 1 kJ mol^{-1}). As a result, the W can freely rotate around its C_2 axis in an effectively quasi-planar CH···OH_2 configuration, as documented by the rotational fine structure of the ν_3 band. W attachment leads to further elongation of the acidic C–H bond of Ad^+ already activated by ionization, causing a large redshift in the corresponding ν_{CH} frequency. However, monohydration is not sufficient to drive intracluster proton transfer from Ad^+ to W, in line with the proton affinities of $C_{10}H_{15}$ and W. From the thermochemical point of view, two to three W molecules are required for this process, which is the basis for functionalization of Ad and other diamondoids in polar solvents via a radical cation mechanism. To this end, the analysis of IRPD spectra of larger $(Ad–W_n)^+$ clusters is currently under way. In general, the CH···O bond in Ad^+–W is comparable to that in monohydrated PAH^+ and H^+PAH cations but weaker than in monohydrates of alkane cations, such as pentane$^+$.

Acknowledgements

This study was supported by Deutsche Forschungsgemeinschaft (DO 729/8).

Conflict of interest

The authors declare no conflict of interest.

Keywords: adamantane cation · C–H activation · hydration · IR spectroscopy · structure elucidation

[1] a) P. v. R. Schleyer, *J. Am. Chem. Soc.* **1957**, *79*, 3292 – 3292; b) R. C. Fort, P. v. R. Schleyer, *Chem. Rev.* **1964**, *64*, 277; c) J. E. Dahl, S. G. Liu, R. M. K. Carlson, *Science* **2003**, *299*, 96 – 99.

[2] a) H. Schwertfeger, A. A. Fokin, P. R. Schreiner, *Angew. Chem. Int. Ed.* **2008**, *47*, 1022 – 1036; *Angew. Chem.* **2008**, *120*, 1038 – 1053; b) P. R. Schreiner, L. V. Chernish, P. A. Gunchenko, E. Y. Tikhonchuk, H. Hausmann, M. Serafin, S. Schlecht, J. E. P. Dahl, R. M. K. Carlson, A. A. Fokin, *Nature* **2011**, *477*, 308; c) W. L. Yang, J. D. Fabbri, T. M. Willey, J. R. I. Lee, J. E. Dahl, R. M. K. Carlson, P. R. Schreiner, A. A. Fokin, B. A. Tkachenko, N. A. Fokina, W. Meevasana, N. Mannella, K. Tanaka, X. J. Zhou, T. van Buuren, M. A. Kelly, Z. Hussain, N. A. Melosh, Z. X. Shen, *Science* **2007**, *316*, 1460 – 1462; d) A. A. Fokin, P. R. Schreiner, *Chem. Rev.* **2002**, *102*, 1551 – 1593; e) L. Wanka, K. Iqbal, P. R. Schreiner, *Chem. Rev.* **2013**, *113*, 3516 – 3604; f) D. F. Blake, F. Freund, K. F. M. Krishnan, C. J. Echer, R. Shipp, T. E. Bunch, A. G. Tielens, R. J. Lipari, C. J. D. Hetherington, S. Chang, *Nature* **1988**, *332*, 611 – 613; g) R. S. Lewis, E. Anders, B. T. Draine, *Nature* **1989**, *339*, 117 – 121; h) O. Pirali, M. Vervloet, J. E. Dahl, R. M. K. Carlson, A. Tielens, J. Oomens, *Astrophys. J.* **2007**, *661*, 919 – 925.

[3] a) A. A. Fokin, P. R. Schreiner, P. A. Gunchenko, S. A. Peleshanko, T. E. Shubina, S. D. Isaev, P. V. Tarasenko, N. I. Kulik, H. M. Schiebel, A. G. Yurchenko, *J. Am. Chem. Soc.* **2000**, *122*, 7317 – 7326; b) M. Mella, M. Freccero, T. Soldi, E. Fasani, A. Albini, *J. Org. Chem.* **1996**, *61*, 1413 – 1422.

[4] a) J. W. Raymonda, *J. Chem. Phys.* **1972**, *56*, 3912; b) S. D. Worley, G. D. Mateescu, C. W. McFarland, R. C. Fort, C. F. Sheley, *J. Am. Chem. Soc.* **1973**, *95*, 7580 – 7586; c) S. X. Tian, N. Kishimoto, K. Ohno, *J. Phys. Chem. A* **2002**, *106*, 6541 – 6553; d) T. Rander, M. Staiger, R. Richter, T. Zimmermann, L. Landt, D. Wolter, J. E. Dahl, R. M. K. Carlson, B. A. Tkachenko, N. A. Fokina, P. R. Schreiner, T. Möller, C. Bostedt, *J. Chem. Phys.* **2013**, *138*, 024310; e) A. Candian, J. Bouwman, P. Hemberger, A. Bodi, A. G. G. M. Tielens, *Phys. Chem. Chem. Phys.* **2018**, *20*, 5399 – 5406.

[5] A. Patzer, M. Schütz, T. Möller, O. Dopfer, *Angew. Chem. Int. Ed.* **2012**, *51*, 4925 – 4929; *Angew. Chem.* **2012**, *124*, 5009 – 5013.

[6] a) A. Gali, T. Demján, M. Vörös, G. Thiering, E. Cannuccia, A. Marini, *Nat. Commun.* **2016**, *7*, 11327; b) T. Xiong, R. Włodarczyk, L. Gallandi, T. Körzdörfer, P. Saalfrank, *J. Chem. Phys.* **2018**, *148*, 044310; c) T. Xiong, P. Saalfrank, *J. Phys. Chem. A* **2019**, *123*, 8871 – 8880.

[7] O. Pirali, V. Boudon, J. Oomens, M. Vervloet, *J. Chem. Phys.* **2012**, *136*, 024310.

[8] a) M. Xie, Y. Matsuda, A. Fujii, *J. Phys. Chem. A* **2016**, *120*, 6351 – 6356; b) T. Endo, Y. Matsuda, A. Fujii, *J. Phys. Chem. Lett.* **2017**, *8*, 4716 – 4719.

[9] a) O. Dopfer, *Int. Rev. Phys. Chem.* **2003**, *22*, 437 – 495; b) O. Dopfer, *Z. Phys. Chem.* **2005**, *219*, 125 – 168; c) E. J. Bieske, O. Dopfer, *Chem. Rev.* **2000**, *100*, 3963 – 3998.

 © 2020 The Authors. Published by Wiley-VCH Verlag GmbH & Co. KGaA, Weinheim

[10] a) O. Dopfer, D. Roth, J. P. Maier, *J. Am. Chem. Soc.* **2002**, *124*, 494 – 502; b) N. Solcà, O. Dopfer, *Angew. Chem. Int. Ed.* **2002**, *41*, 3628 – 3631; *Angew. Chem.* **2002**, *114*, 3781 – 3784; c) N. Solcà, O. Dopfer, *Angew. Chem. Int. Ed.* **2003**, *42*, 1537 – 1540; *Angew. Chem.* **2003**, *115*, 1575 – 1579; d) A. Patzer, S. Chakraborty, N. Solcà, O. Dopfer, *Angew. Chem. Int. Ed.* **2010**, *49*, 10145 – 10148; *Angew. Chem.* **2010**, *122*, 10343 – 10346; e) H. S. Andrei, S. A. Nizkorodov, O. Dopfer, *Angew. Chem. Int. Ed.* **2007**, *46*, 4754 – 4756; *Angew. Chem.* **2007**, *119*, 4838 – 4840; f) H. S. Andrei, N. Solcà, O. Dopfer, *Angew. Chem. Int. Ed.* **2008**, *47*, 395 – 397; *Angew. Chem.* **2008**, *120*, 401 – 403; g) K. Chatterjee, Y. Matsumoto, O. Dopfer, *Angew. Chem. Int. Ed.* **2019**, *58*, 3351 – 3355; *Angew. Chem.* **2019**, *131*, 3389 – 3393; h) K. Chatterjee, O. Dopfer, *Chem. Sci.* **2018**, *9*, 2301 – 2318; i) K. Chatterjee, O. Dopfer, *Phys. Chem. Chem. Phys.* **2017**, *19*, 32262 – 32271.

[11] M. J. Frisch, et al., GAUSSIAN09, Rev. D.01, Gaussian, Inc., Wallingford CT, **2009**.

[12] P. J. Linstrom, W. G. Mallard, NIST Chemistry WebBook, NIST Standards and Technology, Gaithersburg MD, 20899 (http://webbook.nist.gov), **2001**.

[13] a) K. Chatterjee, O. Dopfer, *J. Phys. Chem. A* **2020**, *124*, 1134 – 1151; b) K. Chatterjee, O. Dopfer, *Phys. Chem. Chem. Phys.* **2019**, *21*, 25226 – 25246.

[14] a) P. J. Kelleher, C. J. Johnson, J. A. Fournier, M. A. Johnson, A. B. McCoy, *J. Phys. Chem. A* **2015**, *119*, 4170 – 4176; b) T. Pankewitz, A. Lagutschenkov, G. Niedner-Schatteburg, S. S. Xantheas, Y. T. Lee, *J. Chem. Phys.* **2007**, *126*, 074307.

[15] P. D. Carnegie, B. Bandyopadhyay, M. A. Duncan, *J. Phys. Chem. A* **2008**, *112*, 6237 – 6243.

[16] a) D. J. Goebbert, P. G. Wenthold, *Eur. J. Mass Spectrom.* **2004**, *10*, 837 – 845; b) R. Knochenmuss, O. Cheshnovsky, S. Leutwyler, *Chem. Phys. Lett.* **1988**, *144*, 317 – 323.

[17] a) F. W. Lampe, F. H. Field, J. L. Franklin, *J. Am. Chem. Soc.* **1957**, *79*, 6132 – 6135; b) D. Smith, N. G. Adams, *Int. J. Mass Spectrom. Ion Phys.* **1977**, *23*, 123 – 135; c) W. T. Huntress, R. F. Pinizzotto, J. B. Laudenslager, *J. Am. Chem. Soc.* **1973**, *95*, 4107 – 4115; d) I. Dotan, W. Lindinger, B. Rowe, D. W. Fahey, F. C. Fehsenfeld, D. L. Albritton, *Chem. Phys. Lett.* **1980**, *72*, 67 – 70.

Manuscript received: March 11, 2020
Accepted manuscript online: May 11, 2020
Version of record online: June 4, 2020

 © 2020 The Authors. Published by Wiley-VCH Verlag GmbH & Co. KGaA, Weinheim